

Band restructuring of ordered/disordered blue TiO₂ for visible photocatalyst

Simgeon Oh^{a,c,#}, Ji-Hee Kim^{a,c,#,*}, Hee Min Hwang^{a,c}, Doyoung Kim^{a,c}, Joosung Kim^{a,c}, G.

Hwan Park^{a,b}, Joon Soo Kim^{a,c}, Young Hee Lee^{a,c,*}, Hyoyoung Lee^{a,b,*}

^a*Center for Integrated Nanostructure Physics (CINAP), Institute for Basic Science (IBS), Sungkyunkwan University, Suwon 16419, Korea*

^b*Department of Chemistry, Sungkyunkwan University, Suwon 16419, Korea*

^c*Department of Energy Science, Sungkyunkwan University, Suwon 16419, Korea*

#These authors contribute equally to this work.

*Corresponding authors: kimj@skku.edu (Prof. J.-H. Kim)

leeyoung@skku.edu (Prof. Y. H. Lee)

hyoyoung@skku.edu (Prof. H. Lee)

Abstract

Black TiO₂ with/without noble metal has been proposed for visible photocatalyst, still leaving poor catalyst efficiency. Alternatively, phase-mixed TiO₂ such as anatase and rutile has been commonly used for visible catalysts with the inevitable inclusion of noble metal. Here, we perform a noble metal-free visible photocatalyst blue TiO₂ with type-II band-aligned ordered anatase/disordered rutile structure, via phase-selective reduction with alkali metals. The changed band alignment in this heterostructure was identified by absorption and ultraviolet photoemission spectroscopy, which was further confirmed by transient charge separation. The band alignment of type-I and type-II was clearly restructured by converting from ordered to disordered phase with a prolonged reduction period and as followed light absorbance enhancement also observed. Initiated type-I in a pristine sample, the type-II was organized from disordered rutile phase in 3-day Li-reduction. The type-II disordered rutile TiO₂ heterostructure exhibits a remarkable photocatalytic performance by 55 times higher than

conventional P25 TiO₂ in solar-light driven hydrogen evolution reaction owing to an efficient electron and hole separation of type-II heterojunction. Furthermore, this restructured heterojunction type-II TiO₂ demanded 10 times less Pt amount as a co-catalyst for the comparable photocatalytic performance, compared to Pt decorated type-I pristine anatase/rutile phase-mixed TiO₂.

Keywords: Phase-selective reduction, Phase-mixed TiO₂, Energy band restructuring, Photocatalysis, Hydrogen evolution reaction

1. Introduction

While titanium dioxide (TiO₂) has been widely used as a photocatalyst under UV light, its photocatalytic efficiency is poor even in the presence of a noble metal [1-3]. The visible light solar spectrum is an ideal option to improve the photocatalyst efficiency by ~40% resulting from the solar irradiation intensity compared to 4-5% in UV spectra. For the visible light photocatalyst, a single phased black TiO₂ has been explored with/without noble metals for over a half-century, but required realistic efficiency has not been obtained [4,5]. Afterward, to make a black TiO₂ through whole surface modification of two phase-mixed TiO₂ that is one of renowned photocatalyst material with large surface area, high reduction potential, and efficient charge transfer property from different phase junction structures has been also investigated to improve photocatalytic performance [6,7]. However, this black TiO₂ shows the core-shell structure as a result of the non-phase-selective surface reduction, exposing only the disordered TiO₂ surface. Therefore, its photocatalytic efficiency is still poor mainly due to an easy charge recombination on the disordered shell surface [8]. To overcome the charge recombination issue, two different facet structures of phase-selectively disordered anatase/rutile TiO₂ are previously reported, showing a superior photocatalytic performance than the core-shell structure [9,10].

Nevertheless, in the phase-selectively disordered anatase/rutile TiO_2 facet structure, the relationship between type-I and type-II of the restructured heterojunction band structure and charge transfer efficiency with prolonged reduction time is not clearly understood. For example, the type-II band alignment in the pristine anatase/rutile TiO_2 heterostructure has been proposed for the efficient extraction of electrons and holes [11-13]. In contrast, type-I band alignment has been suggested in photocatalyst systems due to low-energy electron transfer from the rutile to anatase phase [14-16]. To make a worse, for the phase-selectively disordered anatase/rutile TiO_2 , there is no report about the relationship between the band types and charge transfer efficiency. Thus, two questions remain to be resolved: i) which type of band alignment, type-I or type-II, of the anatase/rutile junction and phase-selectively disordered in TiO_2 ? and ii) which phase, anatase or rutile, plays the dominant role for enhancing the charge transfer efficiency through a proper band restructuring?

Here, we report the heterojunction energy band restructuring of selectively ordered/disordered anatase/rutile TiO_2 by tailoring phase-selective reduction. We find obvious type-II heterojunction band structure is organized by 3-day Li-reduction, that the restructured type-II heterojunction is the best choice for the photocatalyst with fast charge transfer between disordered rutile and ordered anatase phase. We were able to tailor the HOMO and LUMO positions by XPS and UPS measurements. Carrier population dynamics clearly confirm by femtosecond transient absorption with the time evolution of band alignment for type-I and type-II. The type-II disordered rutile/ordered anatase TiO_2 heterostructure further demonstrates the best photocatalytic performance in the visible range to date.

2. Experimental

2.1. Chemicals and Materials

The anatase/rutile phase-mixed TiO₂ (Degussa P25) powder was purchased from the Degussa Company. Anatase phase TiO₂, rutile phase TiO₂ powder, lithium metal, sodium metal, chloroplatinic acid, sodium sulfate, and hydrochloric acid were purchased from Merck, Inc. Ethylenediamine was procured from Tokyo Chemical Industry. All reagents were used without further purification.

2.2 Material characterization

The crystalline structures of the samples were analyzed by an X-ray diffraction diffractometer (XRD, Rigaku - Ultima IV) with Cu K α radiation ($\lambda = 0.15418$ nm) at room temperature. All the core-level binding energies were measured by X-ray photoelectron spectroscopy (XPS, VG Microtech - ESCA 2000) with Mg K α ($= 1253.84$ eV) radiation referenced to the C 1s peak of surface adventitious carbon at 284.6 eV. Survey scans and detailed scans of the Ti 2p, O 1s photoelectron peaks were recorded for the samples. In addition, the valence energy band edge of the samples was evaluated by XPS valence band analysis. The optical absorption by the samples was characterized by diffuse reflectance spectroscopy (DRS, Shimadzu-UV-3600) with PTFE used as the white diffuse reflectance standard. The energy band gap of the catalysts was calculated from diffuse reflectance spectra in a Tauc plot. For transient absorption spectroscopy (TAS), the beam from a Ti:sapphire amplifier (Libra, Coherent, USA) with a 1-kHz repetition rate and 80 fs pulse duration was divided into two beams. Here, 95 % of the amplifier drives an optical parametric amplifier (TOPAS Prime, Light Conversion, Lithuania) and is used as a pump beam, which is tuned to 300 nm to excite the TiO₂ sample at an excitation intensity of 1 μ J/pulse. The rest of the amplifier beam produces a white light continuum probe beam in the visible spectral region. Transmission electron microscopy (TEM) was performed using a JEOL-JEM-2100F field-emission instrument at an acceleration voltage of 300 kV. Ultraviolet photoelectron spectroscopy (UPS, Thermo Fisher - ESCALAB 250 Xi) measurement was conducted with UV photons (21.22 eV for He I radiation). To separate the

secondary edges of the samples, a negative potential of 5.0 V was applied for the optimization of Au spectrum. The work function of 5.1 eV was obtained which is a good agreement with previous reports. AC impedance data of the TiO₂ samples were collected using electrochemical impedance spectroscopy (EIS, CH Instruments - CHI660C) with a 0.5 M Na₂SO₄ solution in three-electrode mode with a 3.0 M Ag/AgCl reference electrode. A sinusoidal AC perturbation with a 50 mV amplitude was applied in the frequency range of 10 mHz to 100 kHz. The platinum weight ratio was confirmed by XPS, and the best performing Pt-deposited TiO₂ samples were measured by inductively coupled plasma optical emission spectrometry (ICP-OES, Agilent - 5100).

2.3 Phase-selectively reduced TiO₂ preparation

Phase-selectively reduced TiO₂ was prepared via a modified Birch reduction reaction with different alkali metal-ethylenediamine (EDA) solutions. Single-phase anatase or rutile TiO₂ was used for the phase-selective reduction reaction study, and Degussa P25 served as the standard anatase/rutile phase-mixed TiO₂ for investigation of the phase-selective band restructuring and its photocatalytic performance. Li-EDA and Na-EDA solutions were prepared as follows. Alkali metal (250 mg) was added to a 250 ml round bottom flask. The flask was well sealed with a rubber septum and purged with argon gas for 60 minutes. Subsequently, 50 ml of EDA was injected into the flask with a 50 ml syringe. This solution was vigorously stirred for 24 hours under an argon atmosphere to dissolve the alkali metal. Finally, 500 mg of the respective anatase, rutile, or phase-mixed TiO₂ powder was poured into the prepared solution and stirred for 1-7 days to reduce the TiO₂ crystalline phase. The Li-EDA solution was only used for rutile phase-selective reduction (Li-reduction), and the Na-EDA solution was only used for anatase phase-selective reduction (Na-reduction). These processes are referred to as TiO₂ phase-selective reduction with Li-EDA or Na-EDA solution treatment. The resulting product solution was transferred into a beaker and titrated with 1N HCl aqueous

solution until the solution reached a pH of 7. The final blue TiO₂ powder product was filtrated with a membrane filter, washed with ethanol and deionized water, and dried in a vacuum oven at 40 °C.

2.4 Pt photodeposition

Platinum (Pt)-deposited TiO₂ samples were prepared by photodeposition. Pristine P25 TiO₂ or 3-day Li-reduced phase-mixed TiO₂ was used as the photocatalyst powder, and a 0.001 to 1.0 mM aqueous H₂PtCl₆ solution was added to the powder to deposit different amounts of Pt co-catalyst. TiO₂ powder (100 mg) was added to 100 ml of different concentrations of the Pt precursor solution in a 100 ml glass vial. TiO₂ was well-dispersed by sonication treatment for one hour, and 1 ml of methanol was added as a hole scavenger. The solution-containing vial was well sealed with a quartz cover, and the solution was irradiated with a 100 W UV light (Power Arc UV-100, UV Process Supply, Inc.) under vigorous stirring for one hour. The resulting Pt-deposited TiO₂ sample was filtered with a membrane filter and then washed with ethanol and deionized water.

2.5 Photocatalytic performance estimate

The photocatalytic hydrogen evolution reaction was conducted using a 100 ml Pyrex flask, and AM 1.5 solar light (Oriel Sol 3A Class AAA Solar Simulator, Newport Corp.) was used for the photocatalytic reaction. The newly prepared TiO₂ photocatalyst was soaked in 40 ml of a 3:1 v/v% deionized water/ethanol mixture and sonicated for 24 hours. Then, argon gas was bubbled out for one hour. Simulated 1 sun solar light was irradiated on the prepared samples to generate H₂ gas. The produced H₂ gas was sampled using a 1 ml gas-tight syringe and then analyzed by gas chromatography (YL6500GC, Young Lin Instrument Co. with a molecular sieve 13X column and TCD detector).

3. Results and discussion

3.1. Phase-selective reduction of phase-mixed TiO_2

Our phase-selective reduction of anatase/rutile phase-mixed TiO_2 nanomaterials and their energy band alignment were carefully examined. The reduced phase-mixed TiO_2 samples for phase-selective energy band restructuring are denoted as ordered anatase/disordered rutile (A_o/R_d) and disordered anatase/ordered rutile (A_d/R_o) [17,18]. Degussa P25 served as a standard anatase/rutile phase-mixed TiO_2 in this work. The heterojunction band structure of TiO_2 was considered from the respective band structure of the single-phase disordered (or ordered) anatase and rutile phase TiO_2 (Table S1, Fig. S1, S2, and S3). Representative heterojunction band structures of pristine phase-mixed TiO_2 and reduced TiO_2 are schematically shown in Fig. 1 including type-I with a straddling bandgap for centered ordered rutile and ordered anatase, obvious type-II with a staggered bandgap for disordered rutile and ordered anatase, and reverse type-I for ordered rutile and disordered anatase. The phase-mixed TiO_2 was reduced with Li and Na metals for 7 days. From the carrier dynamics point of view, a type-II heterostructure is ideal for electron transfer from disordered rutile to ordered anatase in the LUMO position and hole transfer back to disordered rutile from ordered anatase in the HOMO position. This is in contrast with a type-I heterostructure, where the transferred electrons and holes recombine with each other, suppressing catalyst efficiency.

The color of the reduced TiO_2 was converted to blue from white after reduction (Fig. S4). The color change is distinct from the genuine black color obtained from conventional hydrogen-reduced TiO_2 since the reduced two phase-mixed TiO_2 shows blue owing to one of the TiO_2 phases kept crystalline structure [19]. The XRD and HRTEM data in Fig. 2 show that an ordered (crystalline) anatase phase is identified with a lattice spacing of 3.53 Å along the (101) direction with a disordered (amorphous) rutile phase after 7 days of Li-reduction (Fig. 2b). Meanwhile, an ordered rutile phase was observed with a lattice spacing of 3.26 Å along the (110) direction with disordered anatase after 7 days of Na-reduction (Fig. 2d). Additional

electron-diffraction FFT pattern information also showed obvious lattice planes of anatase (101) and (110) but amorphous rutile structure FFT pattern with weak anatase overlapped plane for Li-reduction in the inset of Fig. 1b. The FFT pattern of Na-reduction, rutile (110) plane only showed at the rutile particle (see the insets in Fig. 2d). Such structural time evolutions of the reduction were confirmed by XRD (Fig. 2a and 2c). Clear peaks from anatase (101) at 2 theta = 25.3 degree and rutile (110) at 2 theta = 27.5 degree are identified in the phase-mixed TiO₂ sample. The peak ratio of the anatase to rutile phase is large due to the different volumetric ratio of anatase and rutile (80:20) in standard phase-mixed TiO₂ (P25) [20,21]. The peak intensity ratio becomes larger with evolving Li-reduction time owing to the developed disordered rutile phase, which is similarly observed from the full-width-at-half-maximum (FWHM) of the peak (Table S2). In contrast, with Na-reduction, the peak intensity ratio gradually decreases in the anatase phase with evolving reduction time, which is evidence of the emerging disordered anatase phase, whereas the change of the peak intensity is negligible in the rutile phase. Such an emerging disordered anatase phase is reflected by the decreasing peak intensity ratio of I_A/I_R and the FWHM ratio (insets in Fig. 2c and Table S2).

The time evolution of oxygen vacancies and rich Ti³⁺ oxidation states from the disordered phase is confirmed by X-ray photoelectron spectroscopy (XPS) in Fig. 3. The peak position of Ti 2p centered at binding energies of 457.7, 458.3, 463.2, and 464.1 eV corresponds to the Ti³⁺2p_{3/2}, Ti⁴⁺2p_{3/2}, Ti³⁺2p_{1/2} and Ti⁴⁺2p_{1/2}, respectively, which is a good agreement with the previous reports [22,23]. The Ti⁴⁺ oxidation states in the Ti 2p_{3/2} peaks near 458.3 eV are dominant with a minor Ti³⁺ contribution near 457.7 eV in the phase-mixed TiO₂. With Li-reduction, Ti³⁺ oxidation states are distinctly developed after reduction for 7-day, confirming the emergence of a disordered rutile phase with consistent time evolution and the Ti 2p_{1/2} peak also shows same manner (Fig. 3a and inset). The XPS study of reduced single-phase rutile and anatase TiO₂ suggests that the Ti³⁺ oxidation mainly obtained from the rutile phase while the

anatase phase indicates no appreciable oxidation states, maintaining the ordered anatase phase (Fig. S5a and S5c). This trend is also congruent with the developed Ti^{3+} oxidation state or Ti_2O_3 peak in the O 1s spectra. O 1s spectra in Fig. 3a show distinct four oxygen peaks at 529.3, 530.8, 531.8, and 533.2 eV which represents the TiO_2 , oxygen vacancy (Ti_2O_3) and surface oxygen species (-OH, H_2O), respectively [24]. It shows that the oxygen vacancy Ti_2O_3 peak relatively increased as a function of prolonged Li-reduction time. In contrast, in Na-reduction, the Ti^{3+} oxidation states emerge from the disordered anatase phase after 7-day reduction, which is consistent with the related Ti_2O_3 peak in the O 1s spectra (Fig. 3b and inset) [25-27]. A similar trend of oxidation state to phase-mixed TiO_2 was observed in single-phase rutile and anatase TiO_2 study (Fig. S5b and S5d). The apparent oxidation states of Ti^{3+} in the disordered rutile phase with Li-reduction and in the disordered anatase phase with Na-reduction are essential to tailoring the type of band structure and further improving visible light photocatalyst efficiency.

3.2. Identification of energy band restructuring

To tailor the band-type of the ordered/disordered anatase/rutile TiO_2 , we measured the direct bandgap from the Tauc plot via $\sim(\alpha h\nu)^{1/2}$ using UPS and the valence band edge from XPS based on the single-phase TiO_2 (Table S3 and Fig. S3). Fig. 4 exhibits the HOMO and LUMO gaps in terms of reduction time [28-30]. As Li-reduction time is prolonged, the initial HOMO-LUMO gap of 3.0 eV in the ordered rutile phase is narrowed further and the HOMO and LUMO positions are upshifted in the disordered rutile phase [31,32]. Meanwhile, they are nearly constant with a HOMO-LUMO gap of 3.2 eV in the ordered anatase phase, independent of reduction time. The type-I heterostructure is constructed prior to reduction and is converted to a type-II heterostructure after 3-day Li-reduction (Fig. 4a). The HOMO-LUMO gap of disordered rutile is 2.9 eV, which is beneficial for a visible photocatalyst with fast charge transfer. The band type restructuring in Li-reduction is markedly different from that in Na-

reduction. Both HOMO and LUMO positions with an initial HOMO-LUMO gap of 3.2 eV are gradually up-shifted in disordered anatase phase, retaining the type-I heterostructure for up to 1-day with Na-reduction. The type-I is converted to type-II after 2-day reduction by switching the HOMO positions of disordered anatase and ordered rutile. Then, it is further transformed to reverse type-I after 6-day reduction, i.e., the LUMO position of disordered anatase is downshifted below that of ordered rutile (Fig. 4b). The HOMO-LUMO gap is further reduced to 2.7 eV in disordered anatase at 7-day Na-reduction, and band gap decrease was also observed in reduced TiO_2 (Fig. S6).

3.3. Charge extraction in heterostructure

Structural transformation and type-conversion of ordered/disordered anatase/rutile TiO_2 were identified with reduction time evolution, but a comprehensive understanding of the electron-hole separation process in each type of two phase-mixed TiO_2 remains elusive. To monitor the photoexcited charge extraction in each type, we performed femtosecond pump-probe spectroscopy and tracked the differential absorption changes (ΔA) in the time domain [33]. The population density of the anatase phase was normalized to that of the rutile phase within the range of 1,000-2,000 ps near carrier recombination. The normalized kinetics of the anatase and rutile phase in phase-mixed TiO_2 with a type-I heterostructure was observed with a probe photon energy of 3.2 and 3.0 eV, respectively (Fig. 5a). The kinetics of the anatase phase (a probe photon energy of 3.2 eV) decays monotonically through a recombination channel with a maximum population near 0.3 ps [34]. Meanwhile, the maximum population density, ΔA_{\max} , is delayed to ~ 0.8 ps in the rutile phase. The carriers populated in the LUMO and HOMO levels of the anatase phase are transferred to those of the rutile phase, thereby enhancing the carrier density in the rutile phase. The charge transfer occurs efficiently at the interface, which is much shorter than the electron-hole recombination at the nanosecond time scale [35]. While the decay kinetics of each anatase phase is independent of Li-reduction time (Fig. 5b), the

kinetic profiles of the rutile phase are dramatically changed. The population in the rutile phase is enhanced until the 1-day Li-reduction due to the electron and hole transfer (type-I). The population enhancement in the rutile phase becomes mundane from 3 to 7-day reduction. In general, charge separation at the interface of a type-II structure is greatly assisted by a large offset of band restructuring (Fig. 1, Left). However, the defective rutile formed at the interface in the disordered rutile/ordered anatase type-II structure can act as an electron-hole recombination center simultaneously, confirmed by the decreased population at 3 and 7-day reduction (blue dots in Fig. 5d). Moreover, the delayed population of both phases is prolonged when band alignment is restructured from type-I to type-II (Fig. 5b and blue dots in Fig. 5e). In contrast, the kinetic profiles of both phases with Na-reduction show quite different behaviors than Li-reduction (Fig. 5c). The population enhancement in either the anatase or rutile phase via charge transfer is indistinct over the Na-reduction time as well as the type-conversion (red open circles in Fig. 5d). The population density rapidly increases in the anatase phase from reverse type-I at 7-day Na-reduction (Fig. 4b and Fig. 5d). Simultaneously, the maximum population in the rutile phase is delayed by over 1 ps via slow carrier transfer to anatase from rutile (Fig. 5e), originating from disordered anatase with carrier localization centers (ex. oxygen vacancy), which was also confirmed by FTIR (Fig. S7).

3.4. Photocatalytic hydrogen evolution

We evaluated the photocatalytic hydrogen evolution reaction (p-HER) performance with the energy band restructured anatase/rutile phase-mixed TiO₂ as a proof of concept. The p-HER performance is primarily responsible for efficient charge separation which is achieved by proper band alignment and it is expected a type-II heterojunction [36-38]. The p-HER performance examined after confirming the reduction potential of each single-phase TiO₂ for hydrogen reduction by UPS measurement (Fig. S8 and S9). And then the evaluated p-HER performance of TiO₂ samples which are summarized in Fig. 6a and 6b. The ordered/disordered

anatase/rutile TiO_2 reveals enhanced hydrogen production compared to pristine phase-mixed TiO_2 . The disordered rutile phase with 3-day Li-reduction yields the highest p-HER performance (Fig. 6a). The hydrogen evolution rate under simulated 1 sun solar light is $707.03 \mu\text{mol g}^{-1} \text{h}^{-1}$, which is 55 times higher than that of phase-mixed TiO_2 ($12.72 \mu\text{mol g}^{-1} \text{h}^{-1}$). This is mainly attributed to the enhanced light absorption (Fig. S6) and restructured type-II heterojunction structure between anatase and rutile after 3-day Li-reduction (Fig. 4a) for the efficient charge transfer (Fig. 5b). Meanwhile, the p-HER performance decreases rapidly right after 3-day Li-reduction. The degraded performance originates from a heavily defective amorphous structure, which is well comprehended by previous studies [39,40]. The rutile phase is further disordered with a longer Li-reduction time, thus increasing resistance, which is confirmed by the increased equivalent serial resistance determined from electrochemical impedance spectroscopy (Fig. S10a and Table S4) [41]. The p-HER rate with Na-reduction is similar to that of Li-reduction but significantly decreased with higher resistance (Fig. 6b). The large portion of the disordered anatase phase (80%) compared to the disordered rutile phase (20%) in the standard phase-mixed TiO_2 (P25) can be ascribed to the high resistance. Consequently, the p-HER performance decreased rapidly with prolonged Na-reduction time. The resistance becomes saturated after 5-day Na-reduction (Fig. 6b and Fig. S10b), and the LUMO level is reversed into a reverse type-I heterojunction to result in poor charge transfer (Fig. 4b). Rutile phase disordered TiO_2 shows the best p-HER performance at 3-day Li-reduction due to low resistance of the small disordered area, among others, while keeping type-II band alignment for efficient charge transfer (Fig. S11).

To investigate the tangible efficiency of photocatalyst, we explored the p-HER performance of 3-day Li-reduced phase-mixed TiO_2 with the smallest Pt co-catalyst amount. Pt has often served as a noble metal co-catalyst for HER active sites. The Pt-deposited pristine phase-mixed TiO_2 (Pt- TiO_2 , type-I) without reduction shows tenable p-HER performance with an H_2

evolution rate of $5.714 \text{ mmol g}^{-1} \text{ h}^{-1}$ at a 0.03 mM Pt precursor solution. The weight ratio of Pt on the Pt-TiO₂ is 0.46 wt.% versus TiO₂, which is similar to previous reports (Fig. S12 and Table S5) [42-44]. In contrast, with a 10 times more dilute Pt precursor solution (0.003 mM , 0.043 wt.\% of Pt), where the weight ratio of Pt to TiO₂ was analyzed by inductively-coupled-plasma atomic-emission spectroscopy, the p-HER rate of Pt-deposited ordered/disordered phase-mixed TiO₂ with 3-day Li-reduction (Pt-rTiO₂, type-II) shows the best performance ($6.841 \text{ mmol g}^{-1} \text{ h}^{-1}$), which is greater than that of Pt-TiO₂ without reduction (Fig. 6c and Fig. S13).

4. Conclusions

In summary, we perform the band heterojunction restructuring between type-I and type-II in an ordered/disordered anatase/rutile TiO₂. The Li-reduction shows type-I and type-II, and the Na-reduction shows type-I, Type-II, and further reverse type-I heterojunction structure. The HOMO and LUMO levels are determined from the valence band edge using XPS and the bandgap from UPS analysis and restructured heterojunction band structures are confirmed by femtosecond transient absorption spectroscopy. We demonstrated that the type-II rutile phase disordered TiO₂ with Li-reduction is the best candidate for efficient charge transfer and minimum resistance with enhanced light absorption, yielding an HER rate 55 times higher than that of pristine phase-mixed TiO₂. Furthermore, the best photo-HER rate was realized as $6.841 \text{ mmol g}^{-1} \text{ h}^{-1}$ with 10 times smaller Pt amount compared to that in pristine TiO₂ with Pt. This provides plenty of room for phase-selective energy band restructuring to guide the ultimate design of photocatalytic materials with not only a TiO₂ heterostructure but also transition metal chalcogenides and perovskites.

Credit Author Statement

Simgeon Oh carried out all the experimental works. **Hee Min Hwang** and **Joosung Kim** synthesized catalysts. **Hee Min Hwang** performed DRS and band modeling. **Doyoung Kim** performed electrochemical experiments. **G. Hwan Park** performed XRD analysis. **Ji-Hee Kim** and **Joon Soo Kim** carried out the fs-TAS and provide interpretation. **Young Hee Lee** and **Hyoyoung Lee** contributed materials and analysis tools. **Simgeon Oh, Ji-Hee Kim, Young Hee Lee and Hyoyoung Lee** wrote the paper.

Credit Author Statement

The authors declare that they have no known competing financial interests or personal relationships that could have appeared to influence the work reported in this paper.

Acknowledgements

This work was supported by the Institute for Basic Science (IBS-R011-D1).

References

- [1] T. Sreethawong, S. Yoshikawa, Comparative investigation on photocatalytic hydrogen evolution over Cu-, Pd-, and Au-loaded mesoporous TiO₂ photocatalysts, *Catal. Commun.* 6 (2005) 661-668.
- [2] H. Zhou, L. Ding, T.X. Fan, J. Ding, D. Zhang, Q.X. Guo, Leaf-inspired hierarchical porous CdS/Au/N-TiO₂ heterostructures for visible light photocatalytic hydrogen evolution, *Appl. Catal. B Environ.* 147 (2014) 221-228.
- [3] R. Su, R. Tiruvalam, Q. He, N. Dimitratos, L. Kesavan, C. Hammond, J.A. Lopez-Sanchez, R. Bechstein, C.J. Kiely, G.J. Hutchings, F. Besenbacher, Promotion of phenol photodecomposition over TiO₂ using Au, Pd, and Au-Pd nanoparticles, *ACS Nano* 6 (2012) 6284-6292.

- [4] W. Ou, J.Q. Pan, Y.Y. Liu, S. Li, H.L. Li, W.J. Zhao, J.J. Wang, C.S. Song, Y.Y. Zheng, C.R. Li, Two-dimensional ultrathin MoS₂-modified black Ti³⁺-TiO₂ nanotubes for enhanced photocatalytic water splitting hydrogen production, *J. Energy. Chem.* 43 (2020) 188-194.
- [5] Q.J. Xiang, J.G. Yu, M. Jaroniec, Synergetic effect of MoS₂ and graphene as cocatalysts for enhanced photocatalytic H₂ production activity of TiO₂ nanoparticles, *J. Am. Chem. Soc.* 134 (2012) 6575-6578.
- [6] S.J. Yuan, J.J. Chen, Z.Q. Lin, W.W. Li, G.P. Sheng, H.Q. Yu, Nitrate formation from atmospheric nitrogen and oxygen photocatalysed by nano-sized titanium dioxide, *Nat. Commun.* 4 (2013) 2249.
- [7] H. Zhang, X.J. Lv, Y.M. Li, Y. Wang, J.H. Li, P25-graphene composite as a high performance photocatalyst, *ACS Nano* 4 (2010) 380-386.
- [8] E. Han, K. Vijayarangamuthu, J.S. Youn, Y.K. Park, S.C. Jung, K.J. Jeon, Degussa P25 TiO₂ modified with H₂O₂ under microwave treatment to enhance photocatalytic properties, *Catal. Today* 303 (2018) 305-312.
- [9] K. Zhang, L.Y. Wang, J.K. Kim, M. Ma, G. Veerappan, C.L. Lee, K.J. Kong, H. Lee, J.H. Park, An order/disorder/water junction system for highly efficient co-catalyst-free photocatalytic hydrogen generation, *Energy Environ. Sci.* 9 (2016) 499-503.
- [10] H.M. Hwang, S. Oh, J.H. Shim, Y.M. Kim, A. Kim, D. Kim, J. Kim, S. Bak, Y. Cho, V.Q. Bui, T.A. Le, H. Lee, Phase-selective disordered anatase/ordered rutile interface system for visible-light-driven, metal-free CO₂ reduction, *ACS Appl. Mater. Inter.* 11 (2019) 35693-35701.
- [11] D.O. Scanlon, C.W. Dunnill, J. Buckeridge, S.A. Shevlin, A.J. Logsdail, S.M. Woodley, C.R.A. Catlow, M.J. Powell, R.G. Palgrave, I.P. Parkin, G.W. Watson, T.W. Keal, P. Sherwood, A. Walsh, A.A. Sokol, Band alignment of rutile and anatase TiO₂, *Nat. Mater.* 12 (2013) 798-801.

- [12] Y.J. Wang, Q.S. Wang, X.Y. Zhan, F.M. Wang, M. Safdar, J. He, Visible light driven type II heterostructures and their enhanced photocatalysis properties: a review, *Nanoscale* 5 (2013) 8326-8339.
- [13] G. Colon, M.C. Hidalgo, G. Munuera, I. Ferino, M.G. Cutrufello, J.A. Navio, Structural and surface approach to the enhanced photocatalytic activity of sulfated TiO_2 photocatalyst, *Appl. Catal. B Environ.* 63 (2006) 45-59.
- [14] D.Y. Zhang, M.N. Yang, S. Dong, Electric-dipole effect of defects on the energy band alignment of rutile and anatase TiO_2 , *Phys. Chem. Chem. Phys.* 17 (2015) 29079-29084.
- [15] M. Boehme, W. Ensinger, Mixed phase anatase/rutile titanium dioxide nanotubes for enhanced photocatalytic degradation of methylene-blue, *Nano-Micro Lett.* 3 (2011) 236-241.
- [16] D.C. Hurum, A.G. Agrios, K.A. Gray, T. Rajh, M.C. Thurnauer, Explaining the enhanced photocatalytic activity of Degussa P25 mixed-phase TiO_2 using EPR, *J. Phys. Chem. B* 107 (2003) 4545-4549.
- [17] C.T.K. Nguyen, N.Q. Tran, S. Seo, H. Hwang, S. Oh, J.M. Yu, J.S. Lee, T.A. Le, J. Hwang, M. Kim, H. Lee, Highly efficient nanostructured metal-decorated hybrid semiconductors for solar conversion of CO_2 with almost complete CO selectivity, *Mater. Today* 35 (2020) 25-33.
- [18] Y. Kim, H.M. Hwang, L. Wang, I. Kim, Y. Yoon, H. Lee, Solar-light photocatalytic disinfection using crystalline/amorphous low energy bandgap reduced TiO_2 , *Sci. Rep.* 6 (2016) 25212.
- [19] X.B. Chen, L. Liu, F.Q. Huang, Black titanium dioxide (TiO_2) nanomaterials (vol 44, pg 1861, 2015), *Chem. Soc. Rev.* 44 (2015) 2019-2019.
- [20] G. Hyett, M. Green, I.P. Parkin, X-ray diffraction area mapping of preferred orientation and phase change in TiO_2 thin films deposited by chemical vapor deposition, *J. Am. Chem. Soc.* 128 (2006) 12147-12155.
- [21] R. Quesada-Cabrera, A. Mills, C. O'Rourke, Action spectra of P25 TiO_2 and a visible light

absorbing, carbon-modified titania in the photocatalytic degradation of stearic acid, *Appl. Catal. B Environ.* 150 (2014) 338-344.

[22] Y. Park, H. Sim, M. Jo, G.Y. Kim, D. Yoon, H. Han, Y. Kim, K. Song, D. Lee, S.Y. Choi, J. Son, Directional ionic transport across the oxide interface enables low-temperature epitaxy of rutile TiO_2 , *Nat. Commun.* 11 (2020) 1401.

[23] J.Y. Zheng, Y.H. Lyu, R.L. Wang, C. Xie, H.J. Zhou, S.P. Jiang, S.Y. Wang, Crystalline TiO_2 protective layer with graded oxygen defects for efficient and stable silicon-based photocathode, *Nat. Commun.* 9 (2018) 3572.

[24] S. Benkoula, O. Sublemontier, M. Patanen, C. Nicolas, F. Sirotti, A. Naitabdi, F. Gaie-Levrel, E. Antonsson, D. Aureau, F.X. Ouf, S.I. Wada, A. Etcheberry, K. Ueda, C. Miron, Water adsorption on TiO_2 surfaces probed by soft X-ray spectroscopies: bulk materials vs. isolated nanoparticles, *Sci. Rep.* 5 (2015) 15088.

[25] S. Oh, H. Ha, H. Choi, C. Jo, J. Cho, H. Choi, R. Ryoo, H.Y. Kim, J.Y. Park, Oxygen activation on the interface between Pt nanoparticles and mesoporous defective TiO_2 during CO oxidation, *J. Chem. Phys.* 151 (2019) 234716.

[26] G. Ou, Y.S. Xu, B. Wen, R. Lin, B.H. Ge, Y. Tang, Y.W. Liang, C. Yang, K. Huang, D. Zu, R. Yu, W.X. Chen, J. Li, H. Wu, L.M. Liu, Y.D. Li, Tuning defects in oxides at room temperature by lithium reduction, *Nat. Commun.* 9 (2018) 1302.

[27] M.M. Ye, J. Jia, Z.J. Wu, C.X. Qian, R. Chen, P.G. O'Brien, W. Sun, Y.C. Dong, G.A. Ozin, Synthesis of black TiO_x nanoparticles by Mg reduction of TiO_2 nanocrystals and their application for solar water evaporation, *Adv. Energy Mater.* 7 (2017) 1601811.

[28] T.C. Wei, Y.N. Zhu, X.Q. An, L.M. Liu, X.Z. Cao, H.J. Liu, J.H. Qu, Defect modulation of Z-scheme $\text{TiO}_2/\text{Cu}_2\text{O}$ photocatalysts for durable water splitting, *ACS Catal.* 9 (2019) 8346-8354.

[29] C. Caro, K. Thirunavukkarasu, M. Anilkumar, N.R. Shiju, G. Rothenberg, Selective

autoxidation of ethanol over titania-supported molybdenum oxide catalysts: structure and reactivity, *Adv. Synth. Catal.* 354 (2012) 1327-1336.

[30] Y.Q. Yang, L.C. Yin, Y. Gong, P. Niu, J.Q. Wang, L. Gu, X.Q. Chen, G. Liu, L.Z. Wang, H.M. Cheng, An unusual strong visible-light absorption band in red anatase TiO_2 photocatalyst induced by atomic hydrogen-occupied oxygen vacancies, *Adv. Mater.* 30 (2018) 1704479.

[31] X.B. Chen, L. Liu, P.Y. Yu, S.S. Mao, Increasing solar absorption for photocatalysis with black hydrogenated titanium dioxide nanocrystals, *Science* 331 (2011) 746-750.

[32] K. Zhang, J.H. Park, Surface localization of defects in black TiO_2 : enhancing photoactivity or reactivity, *J. Phys. Chem. Lett.* 8 (2017) 199-207.

[33] L. Collado, A. Reynal, F. Fresno, M. Barawi, C. Escudero, V. Perez-Dieste, J.M. Coronado, D.P. Serrano, J.R. Durrant, V.A.D. O'Shea, Unravelling the effect of charge dynamics at the plasmonic metal/semiconductor interface for CO_2 photoreduction, *Nat. Commun.* 9 (2018) 4986.

[34] M. Sachs, E. Pastor, A. Kafizas, J.R. Durrant, Evaluation of surface state mediated charge recombination in anatase and rutile TiO_2 , *J Phys Chem Lett* 7 (2016) 3742-3746.

[35] Y.N. Wang, Y.L. Shi, C.Y. Zhao, Q.J. Zheng, J. Zhao, Photogenerated carrier dynamics at the anatase/rutile TiO_2 interface, *Phys. Rev. B* 99 (2019) 165309.

[36] D. Sarkar, C.K. Ghosh, S. Mukherjee, K.K. Chattopadhyay, Three dimensional $\text{Ag}_2\text{O}/\text{TiO}_2$ type-II (p-n) nanoheterojunctions for superior photocatalytic activity, *ACS Appl. Mater. Inter.* 5 (2013) 331-337.

[37] S. Cho, J.W. Jang, J. Kim, J.S. Lee, W. Choi, K.H. Lee, Three-dimensional type II ZnO/ZnSe heterostructures and their visible light photocatalytic activities, *Langmuir* 27 (2011) 10243-10250.

[38] X.M. Jia, J. Cao, H.L. Lin, M.Y. Zhang, X.M. Guo, S.F. Chen, Transforming type-I to type-II heterostructure photocatalyst via energy band engineering: a case study of I-BiOCl/I-

BiOBr, *Appl. Catal. B Environ.* 204 (2017) 505-514.

[39] A. Cappelli, E. Piccinini, F. Xiong, A. Behnam, R. Brunetti, M. Rudan, E. Pop, C. Jacoboni, Conductive preferential paths of hot carriers in amorphous phase-change materials, *Appl. Phys. Lett.* 103 (2013) 083503.

[40] H.S.P. Wong, S. Raoux, S. Kim, J.L. Liang, J.P. Reifenberg, B. Rajendran, M. Asheghi, K.E. Goodson, Phase change memory, *P. IEEE* 98 (2010) 2201-2227.

[41] A. Noori, M.F. El-Kady, M.S. Rahmanifar, R.B. Kaner, M.F. Mousavi, Towards establishing standard performance metrics for batteries, supercapacitors and beyond, *Chem. Soc. Rev.* 48 (2019) 1272-1341.

[42] T.Q. Lin, C.Y. Yang, Z. Wang, H. Yin, X.J. Lu, F.Q. Huang, J.H. Lin, X.M. Xie, M.H. Jiang, Effective nonmetal incorporation in black titania with enhanced solar energy utilization, *Energy Environ. Sci.* 7 (2014) 967-972.

[43] M. Xiao, L. Zhang, B. Luo, M.Q. Lyu, Z.L. Wang, H.M. Huang, S.C. Wang, A.J. Du, L.Z. Wang, Molten-salt-mediated synthesis of an atomic nickel co-catalyst on TiO₂ for improved photocatalytic H₂ evolution, *Angew. Chem. Int. Ed.* 59 (2020) 7230-7234.

[44] S. Hoang, Y.B. Guo, A.J. Binder, W.X. Tang, S.B. Wang, J. Liu, H. Tran, X.X. Lu, Y. Wang, Y. Ding, E.A. Kyriakidou, J. Yang, T.J. Toops, T.R. Pauly, R. Ramprasad, P.X. Gao, Activating low-temperature diesel oxidation by single-atom Pt on TiO₂ nanowire array, *Nat. Commun.* 11 (2020) 1062.

Figures

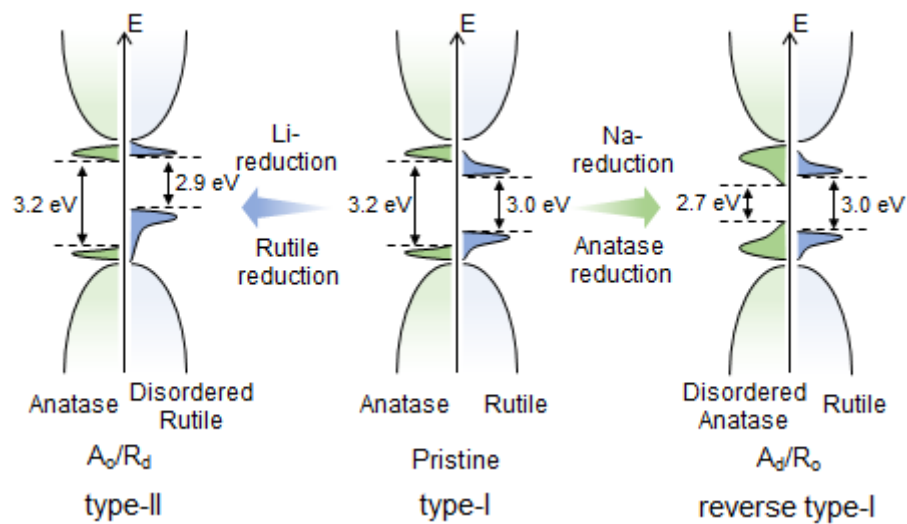


Fig. 1. Heterojunction band alignments of pristine phase-mixed TiO_2 , band restructured 7-day Li-reduction (A_o/R_d , Left), 7-day Na-reduction (A_d/R_o , Right), respectively.

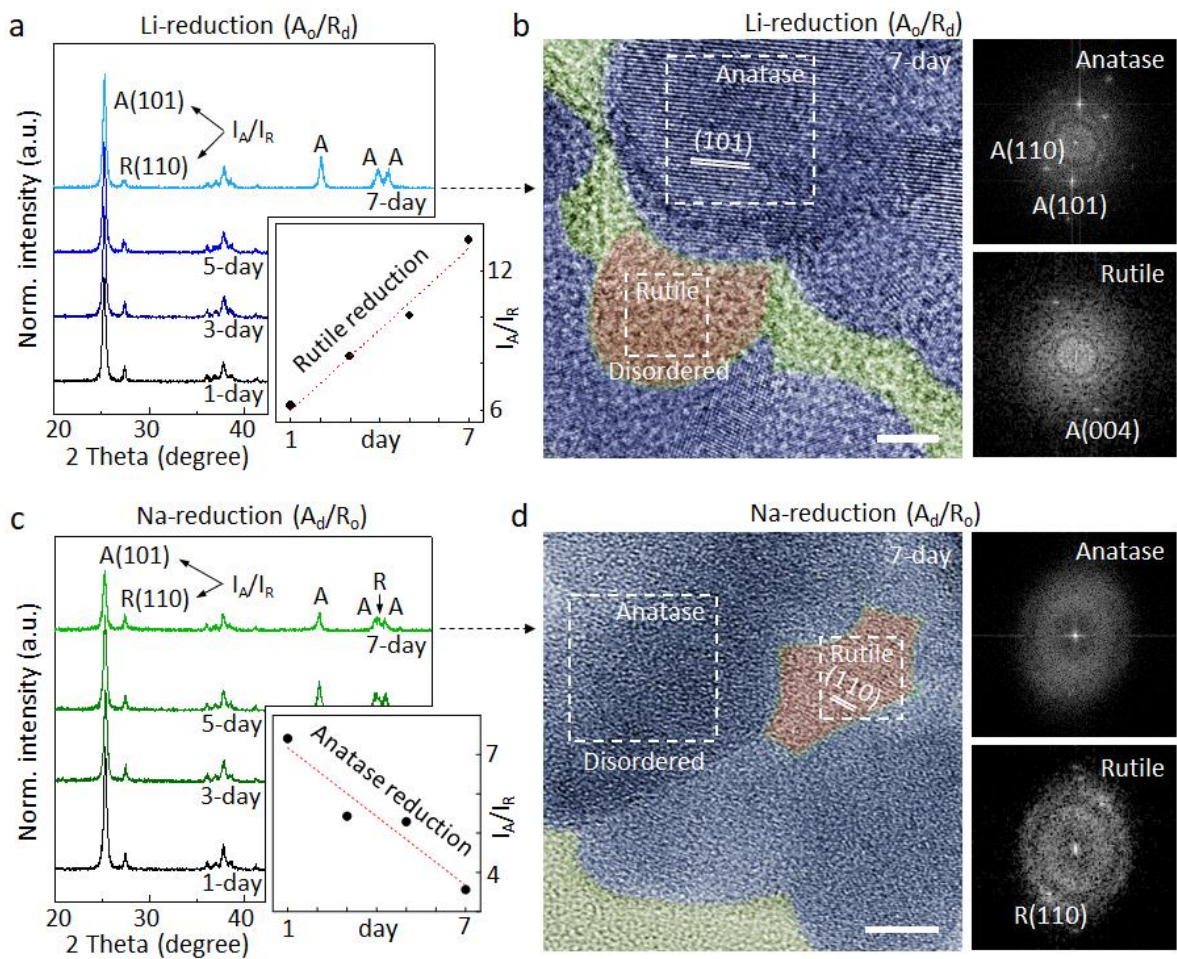


Fig. 2. Crystal and chemical structural characterization of alkali metal-treated phase-mixed TiO_2 . XRD patterns of (a) 7-day Li-reduction (A_0/R_d) and (c) 7-day Na-reduction (A_d/R_0). Inset: Variation of I_A/I_R values corresponding to the peak intensity ratio of anatase (101) to rutile (110). HRTEM images of (b) 7-day Li-reduction (A_0/R_d) and (d) 7-day Na-reduction (A_d/R_0). Scale bars are 5 nm. Inset: Electron-diffraction FFT patterns of anatase and rutile phases.

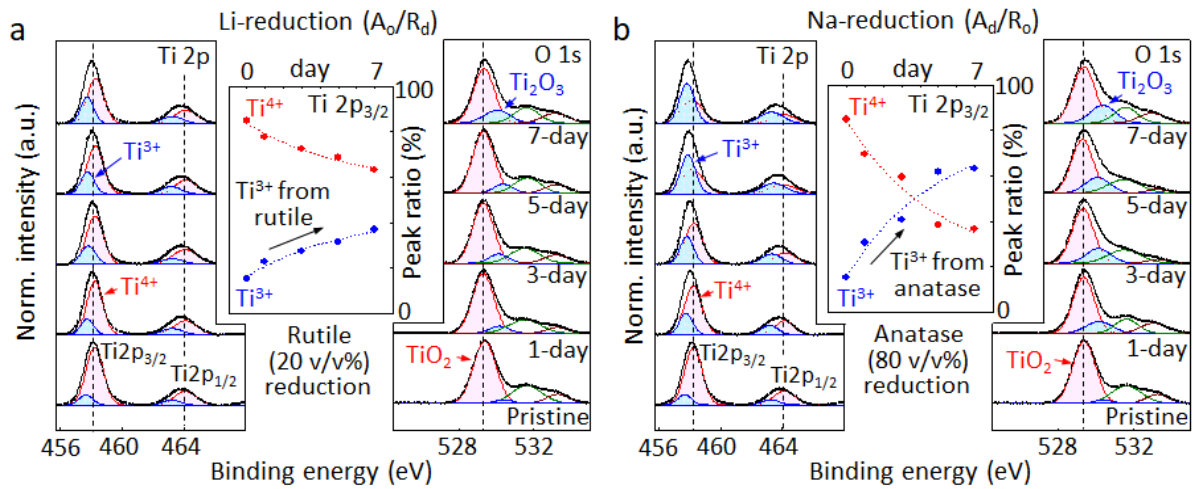


Figure 3. XPS core-level spectra of Ti 2p and O 1s from (a) Li-reduced (A_o/R_d) and (b) Na-reduced (A_d/R_o) phase-mixed TiO_2 . Inset: Deconvoluted peak ratio of Ti^{4+} and Ti^{3+} from the $\text{Ti} 2\text{p}_{3/2}$ peak with Li- and Na-reduction time evolution.

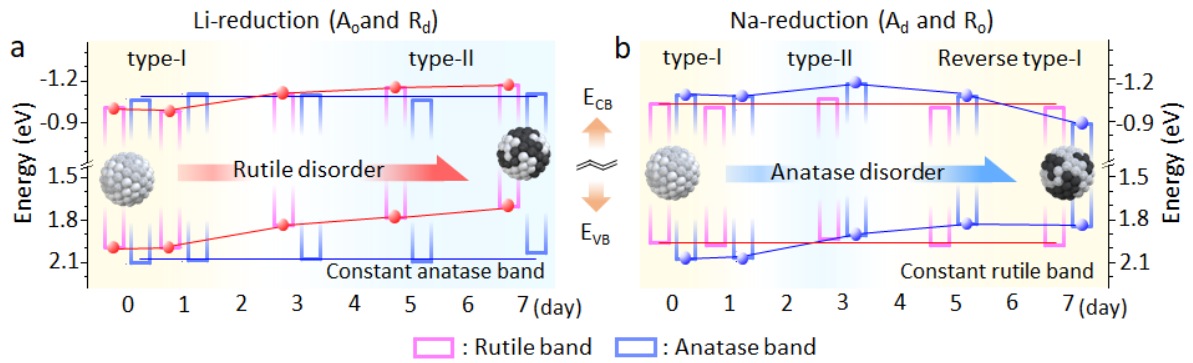


Figure 4. Restructured energy band positions of phase-mixed TiO_2 with the reduction time evolution. (a) Heterojunction band structures of ordered anatase and disordered rutile TiO_2 interface with Li-reduction. (b) Heterojunction band structures of disordered anatase and ordered rutile TiO_2 interface with Na-reduction.

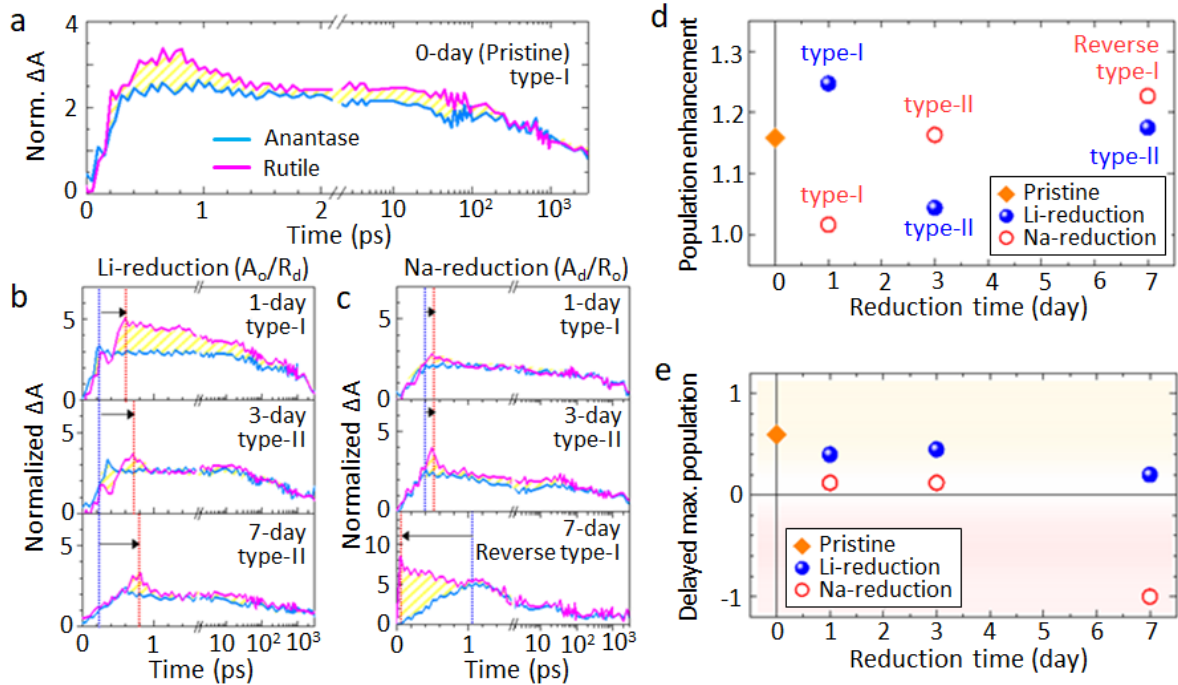


Figure 5. Femtosecond transient absorption spectra of phase-mixed TiO_2 . Normalized femtosecond transient absorption spectra of (a) pristine phase-mixed TiO_2 , (b) Li-reduced (A_o/R_d) and (c) Na-reduced (A_d/R_o) phase-mixed TiO_2 . The 300 nm pump photon excitation energy applied. (d) Population enhancement tendency. (e) Delayed maximum population.

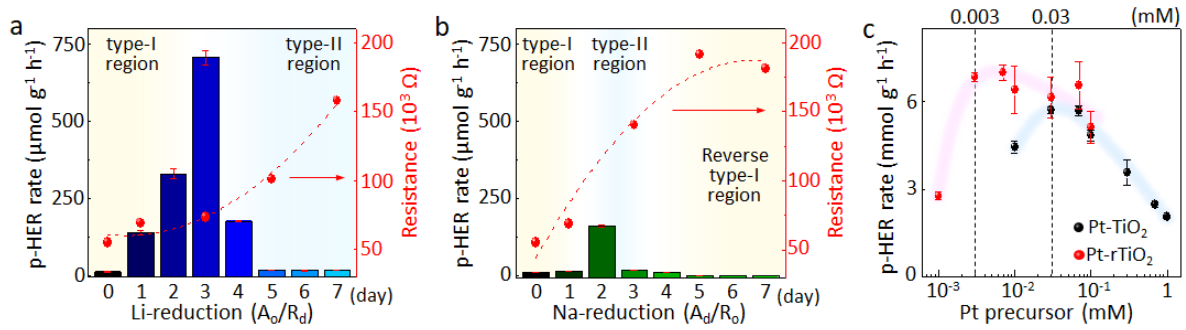


Figure 6. Photocatalytic hydrogen evolution reaction (p-HER). The p-HER rate and equivalent serial resistance of (a) Li-reduced (A_o/R_d) and (b) Na-reduced (A_d/R_o) phase-mixed TiO_2 . (c) The p-HER rates of Pt-TiO₂ and Pt-rTiO₂ with a 10 times smaller amount of Pt co-catalyst.